Thermoelectric Properties of *p*- and *n*-type $Eu_5Sn_2As_6$

Kasey P. Devlin, Braulio Gomez, and Susan M. Kauzlarich*

Department of Chemistry, University of California, One Shields Avenue, Davis, California 95616, United States

Contribution for the special issue to celebrate the 60th birthday of Caroline Röhr

Abstract

$Eu_5Sn_2As_6$ is a Zintl phase crystalizing in the orthorhombic space group *Pbam* with one-dimensional chains of corner-shared $SnAs_4$ tetrahedra running in the *c* direction. $Eu_5Sn_2As_6$ has an impressive room temperature Seebeck of > 100 μV/K and < - 100 μV/K at 600 K crossing from *p*- to *n*-type at 650 K. The maximum thermoelectric figure of merit, *zT*, for $Eu_5Sn_2As_6$ is small (0.075), comparable to that of the Zintl phase $Ca_5Al_2Sb_6$ whose thermoelectric performance was improved by doping Na onto the Ca sites. In this study, we show that the thermoelectric properties of $Eu_5Sn_2As_6$ can be improved by doping with K or La. The series $Eu_{5-x}K_xSn_2As_6$ provides an increase in maximum *zT* of 0.22 for x = 0.15 due to a decrease resistivity while the onset of bipolar conduction systematically increases in temperature. Upon La doping, $Eu_{5-x}La_xSn_2As_6$ results in a new *n*-type Zintl phase across the temperature range of 300 – 800 K.

INTRODUCTION

$Eu_5Sn_2As_6$ exists in the $A_5M_2Pn_6$ family of compounds crystallizing in the $Ca_5Sn_2As_6$ structure type (space group *Pbam*).[1] This structure type has been found to accommodate a variety of atoms in the crystallographic sites: A can be Sr, Eu, and Ca, M is Sn, and Pn can be P and As.[1–4] The $A_5M_2Pn_6$ composition is known to crystallize in four distinct structure types: $Ca_5Ga_2As_6$,[5] $Ca_5Al_2Bi_6$,[6] $Ca_5Sn_2As_6$,[2,4] and $Sr_5Al_2Sb_6$.[7] These structure types have been studied in detail and are similar, only differing in cation coordination environment.[1,2,4–6,8] The $Eu_5Sn_2As_6$ structure crystallizes in the $Ca_5Sn_2As_6$ structure type of the *Pbam* space group, **Figure 1**. $Ca_5Ga_2As_6$ has a $[Ga_2As_6]^{10-}$ chain that can be described as two bridging single chains of $GaAs_4$ tetrahedra that are linked through As corners and are further connected via an As-As bond to form a double-chain. Whereas the $Ca_5Sn_2As_6$ structure type has two discrete $[SnAs_3]$ chains made of corner shared $SnAs_4$ tetrahedra. The $Sr_5Al_2Sb_6$ has the largest difference from other $A_5M_2Pn_6$ structures as the primitive cell contains double the number of atoms and $Sr_5Al_2Sb_6$ has oscillating chains along the c-axis due to alternating

corner- and edge-sharing between the $AlSb_4$ tetrahedra. The electron counting of these $A_5M_2Pn_6$ materials can be understood as consisting of 5 isolated Eu^{2+} atoms, 2 Sn^{4+} atoms, and 6 As^{3-} atoms: $[Sr^{2+}]_5[Sn^{4+}]_2[As^{3-}]_6$.

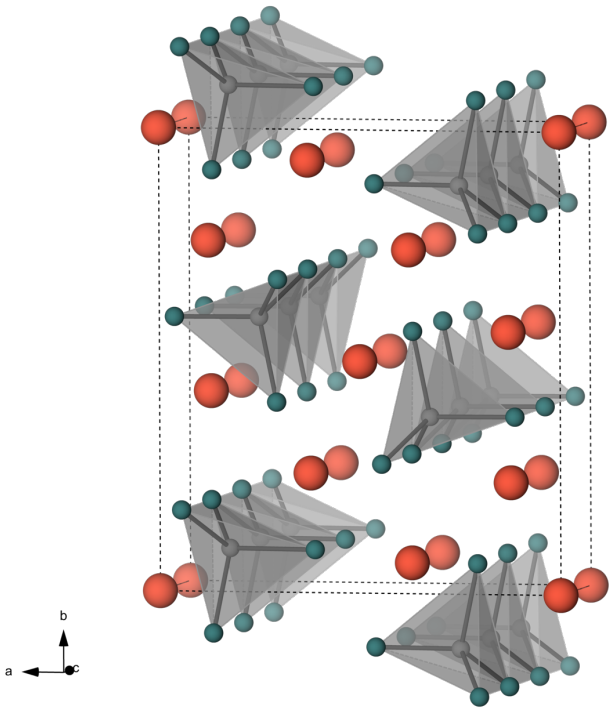

Figure 1. $Eu_5Sn_2As_6$ structure viewed between the *a*- and *c*- axes where Eu is indicated in orange, Sn is grey, and As is teal.

Of the various compounds of the $Ca_5Ga_2As_6$ structure type, $Ca_5Al_2Sb_6$ has been one of the most studied to date for thermoelectric properties.[9,10] In the $Ca_5Al_2Sb_6$ phase the A site has been substituted with Na and the M site has been substituted with Zn and Mn.[9] In all three studies, the *zT* of the material was improved from the > 0.1 *zT* of the parent compound to near 0.6 at ~ 900 K. Additionally, all of the $Ca_5Al_2Sb_6$ site substitutions have led to *p*-type Zintl phases. Most Zintl phases have been observed as *p*-type semiconductors; however, attempts have been made to substitute *p*-type structures into *n*-type semiconductors.[11,12] In addition to experimental attempts at doping *p*-type structure to be *n*-type, Gorai et. al. investigated the use of computational defect diagrams as a way to guide the synthesis of substituted *n*-type Zintl phases.[13] The substitution of Zintl phases from *p*- to *n*-type semiconductors is limited by the native defects of a material having low formation energy; this type of acceptor defect, or "electron killer", can make

it difficult or impossible to dope a material *n*-type.[13] Although Zintl phases are difficult to substitute to be *n*-type semiconductors, there are a few promising Zintl phases that are inherently *n*-type or can be further substituted *n*-type: $Ca_5Al_2Sb_6$,[10] $KGaSb_4$,[14,15] $KAlSb_4$,[16,17] $Zr_3Ni_3Sb_4$,[18] $Ca_{11}Sb_{10}$.[19] $Eu_5Sn_2As_6$ is of interest as a candidate to become an *n*-type Zintl phase due to the low temperature *p*-type to *n*-type transition of the material.

The thermoelectric properties of the $Eu_5Sn_2As_6$ compound were studied by Wang et al. and found that the material exhibited a *p*-type to *n*-type transition at ~ 500 K.[1] This work examines the both *p*-type doping and *n*-type doping of the $Eu_5Sn_2As_6$ material.

EXPERIMENTAL

Synthesis

Bulk samples were produced in 3 g batches. Eu, La/K, Sn, and As were ball milled in a 5 mL WC lined grinding vial with two ~ 4 g WC balls on the desired stoichiometry. The grinding vial was sealed in two polybags under argon and mechanically agitated in a SPEX 8000M mixer mill. The samples were milled for 2 x 30 minutes with scraping in between millings. The samples are sealed in 3.5" of Nb tubing and jacketed under vacuum in quartz. The tubes were heated to 650 °C, held for 168 hours, and allowed to cool to ambient temperature. The temperature 650 °C was chosen because it is 2/3 the reported decomposition temperature (977 °C).[1]

Spark Plasma Sintering

The powdered samples were consolidated into dense pellets using a Dr. Sinter-Lab SPS-211LX. The powders were sieved (100-mesh) and loaded into graphite dies with an inner diameter of 12.7 mm, a height of 30 mm, and a 30 mm outer diameter. A hole in the die for thermocouple placement allowing for precise control over the temperature profile during the sintering process. The samples were compacted by applying a force of 2 kN under vacuum, and then heated to 550 °C in 9 minutes. The reaction is subsequently heated to 580 °C in 1 min and allowed to dwell for 10 min. At 500 °C the force is increased to 8 kN before reaching the maximum temperature.

Powder X-ray Diffraction

Powder X-ray diffraction (PXRD) was performed on pre-SPSed ground powders, made from the reaction products, loaded onto a zero-background holder. PXRD was collected with a Bruker D8 Eco Advance Powder X-ray diffractometer with Cu Kα radiation (λ = 1.54060 Å) with a 2θ range from 8° to 50° or 8° to 80° with a step size of ~0.02° and a scan rate of 1s/step utilizing a Lynx-EX detector.

Thermoelectric Properties

Thermal diffusivity (D) measurement was conducted on the pellet obtained from SPS from 300 K to 575 K on a Netzsch LFA-457 unit. The pellet surfaces were polished flat and parallel and coated with graphite. The measurement was conducted under a dynamic argon atmosphere with a flow rate of 50 mL/min. Thermal conductivity was calculated using the equation $\kappa = D \times \rho \times C_p$ where heat capacity was estimated using Dulong-Petite. Lattice thermal conductivity was calculated by subtracting the electronic contribution of the thermal conductivity from the total thermal conductivity. The electronic contribution of the thermal conductivity was calculated using the Wiedemann-Franz law where the Lorenz number was approximated to 1.538×10^{-8} K from the parent compound, $Eu_5Sn_2As_6$.

Seebeck and electrical resistivity measured at NASA's Jet Propulsion Laboratory were performed on 12.7 mm SPSed pellets from 300 K to 825 K. The Seebeck coefficient was measured under high vacuum using a custom-fabricated apparatus using the light-pulse method with tungsten-niobium thermocouples.[20] Temperature dependent Hall coefficient and electrical resistivity were measured using the Van der Pauw method with a 0.8 T magnet with tungsten pressure contact probes at a heating rate of 180 K/hr using a custom-fabricated instrument.[21] The experimental data were fit with a polynomial function used to calculate zT and are plotted versus temperature.

A Linseis LSR-3 unit was employed to measure the Seebeck coefficient and electrical resistivity via a four-probe method from 335 K to 710 K under a helium atmosphere on a bar-shaped sample. The sample which had been previously measured on the LFA instrument was cut into an approximately 2 × 2 × 10 mm bar using a Buehler diamond saw and polished before measurement. The probe distance was 8 mm. All thermoelectric data were fit with a multi-order polynomial to calculate zT and are plotted versus temperature.

Room Temperature Resistivity

Room temperature resistivity measurements were taken on a home-built system utilizing the Van Der Pauw technique. The current is supplied by Keithley 224 Programmable Current Source and the voltage is measured by a Keithley 182 Sensitive Digital Voltmeter. The piano wire leads are attached to the sample via screw apparatus to apply tension.

Results and Discussions

Thermoelectric Properties

The PXRD patterns of $Eu_{5-x}A_xSn_2As_6$ (A = La; K; x = 0-0.2) showing a section from 31.5° to 34° is provided in **Figure 2**. The PXRD data for the samples from 20° to 50° are illustrated in **Figure S1**, and the Rietveld refinement plots are depicted in **Figures S2A – S2H** with the results summarized in **Table S1**. The main impurity phase that is identified in the samples is Eu_2O_3, at amounts less than ~2 weight %.

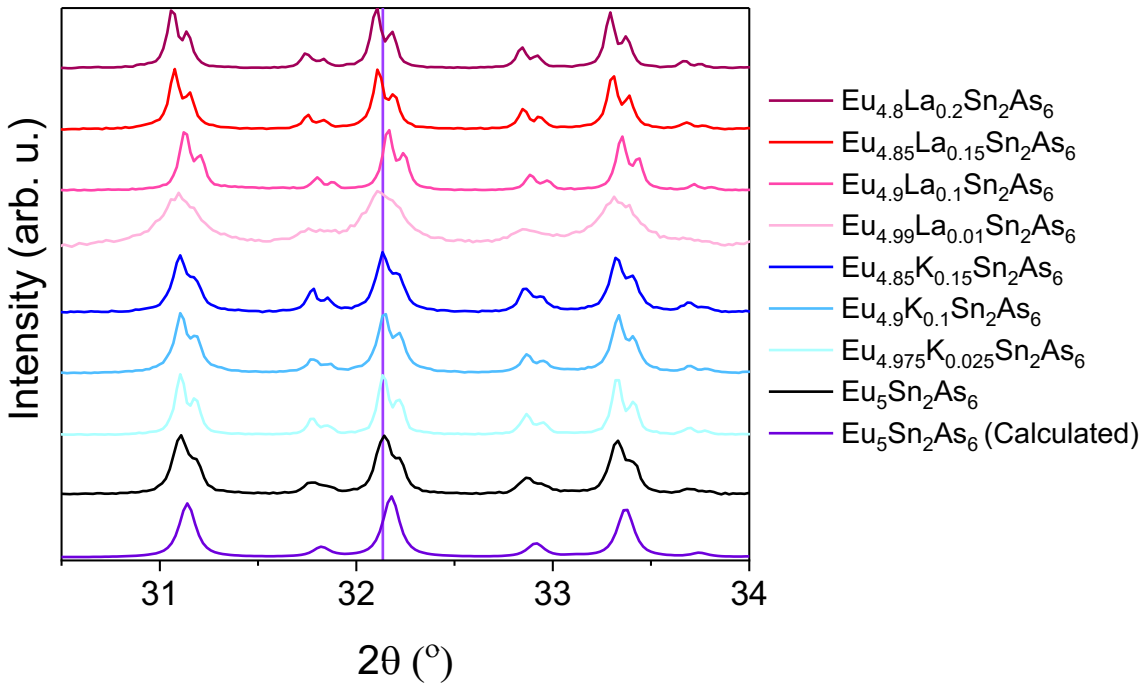

Figure 2. The PXRD patterns of all bulk samples from 31.5° to 34° compared to the calculated $Eu_5Sn_2As_6$ and Eu_2O_3 patterns. The patterns include both $K\alpha_1$ and $K\alpha_2$. The $Eu_5Sn_2As_6$ peaks are (3 1 1), (4 2 0), (2 3 1), (1 5 0) and (0 4 1). The purple line indicates the peak position of the parent compounds (2 3 1) peak.

The thermal conductivity is illustrated in **Figure 3A**, where all the measured compounds are plotted together. In **Figure 3B**, $Eu_{5-x}K_xSn_2As_6$ (x = 0.025, 0.1, and 0.15) are plotted against the parent compound. The thermal conductivity of $Eu_5Sn_2As_6$ is slightly lower, but in good agreement with the previously published values.[1] For the *p*-substituted series, the thermal conductivity of $Eu_{5-x}A_xSn_2As_6$ is largely unchanged. The La substituted series is shown in **Figure 3C**; with low amounts of La added (x = 0.01 and 0.1) there is very little change in the thermal conductivity; however, at the higher amounts (x = 0.15 and 0.2) the thermal conductivity is similar at low temperatures, but the slight upturn at high, ~550 K, is removed. This could be an indication that bipolar conduction is minimized with the higher doping. In **Figure 3D**, the lattice thermal conductivity is calculated, but has almost no change from the total thermal conductivity indicating that the electrical portion of the thermal conductivity has little to no effect on the total thermal conductivity.

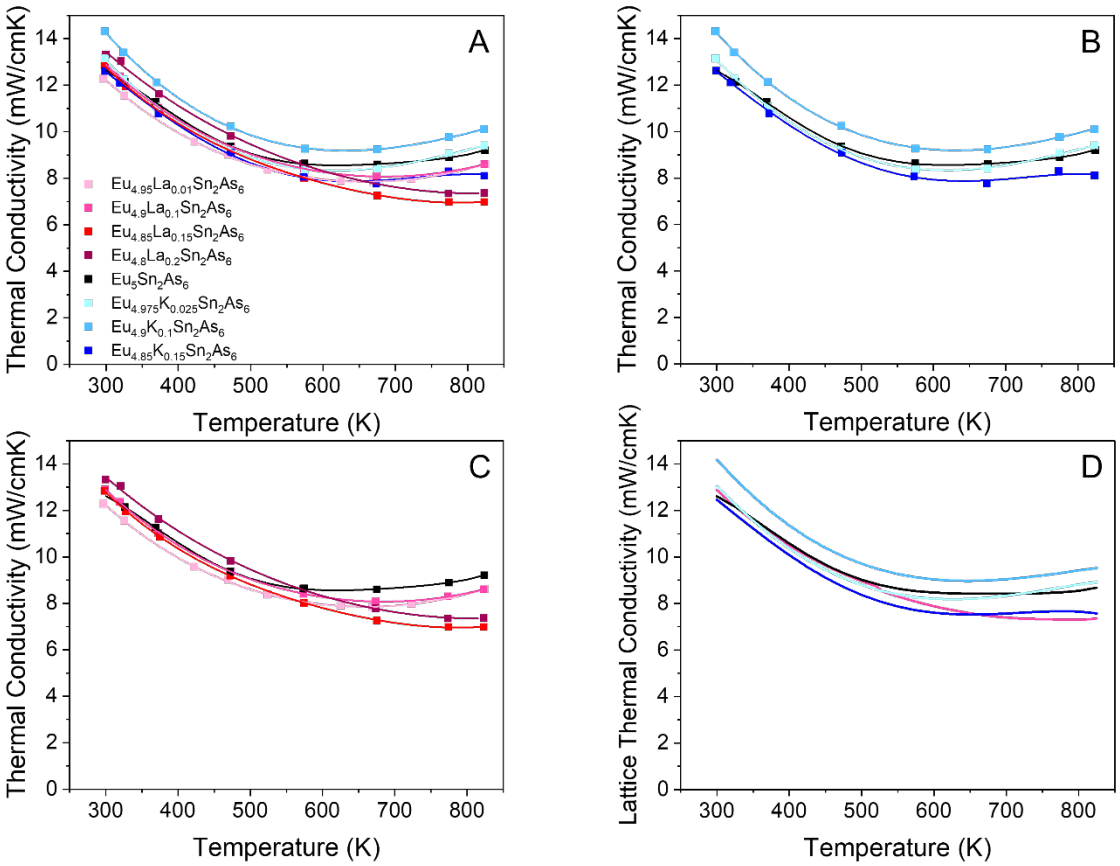

Figure 3. Thermal Conductivity of $Eu_{5-x}A_xSn_2As_6$ (A = K, La) compounds where squares represent experimental data and lines are polynomial fits: (A) All compounds, (B) K-substituted compounds, (C) La-substituted compounds, and (D) Lattice thermal conductivity for available samples.

The biggest challenge facing the thermoelectric properties of $Eu_5Sn_2As_6$ is the very large electrical resistivity. At room temperature the electrical resistivity is > 400 mΩ-cm. This is slightly higher than what has been previously reported,[1] but consistent with the slightly lower thermal conductivity observed. Small differences in the defect concentration can account for these differences. **Figure 4A** shows resistivity versus temperature for the series $Eu_{5-x}K_xSn_2As_6$ (x = 0.025, 0.1, and 0.15). These compositions have decreasing resistivity with increasing K content. **Table 1** provides the additional phases of $Eu_{5-x}La_xSn_2As_6$ (x = 0.01, 0.1, 0.15, and 0.2) and these show an initial increase in resistivity. Beyond x = 0.1 the resistivity is significantly decreased. Most of the samples were measured at the Jet Propulsion Laboratory due to the electrical resistivity being too high to measure with the Linseis LSR3 instrument; however, the $Eu_{4.8}La_{0.2}Sn_2As_{12}$ sample was measured on the Linseis LSR3, due to the significant decrease in electrical resistivity. The $Eu_{4.85}La_{0.15}Sn_2As_{12}$ sample was not measured beyond thermal conductivity.

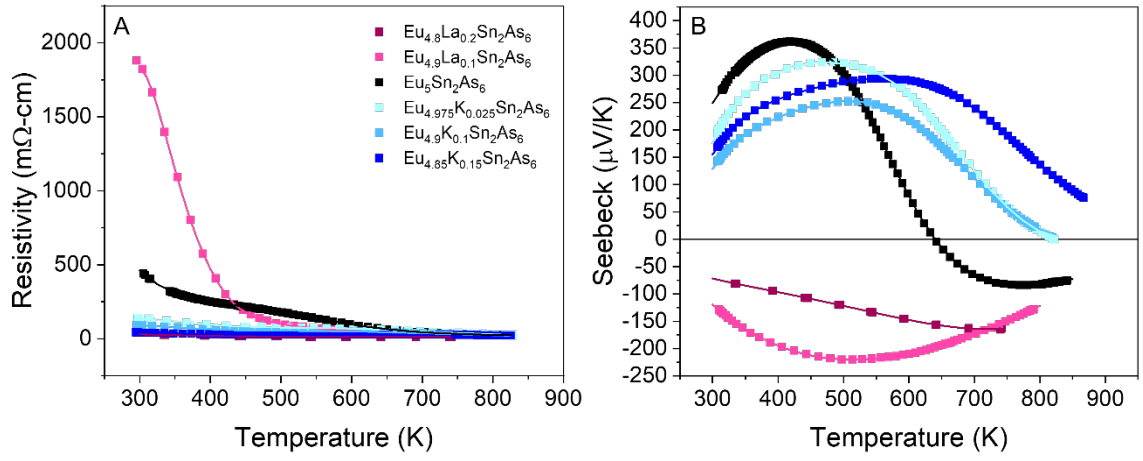

Figure 4. (A) Electrical resistivity of select $Eu_{5-x}A_xSn_2As_6$ (A = K, La) compounds where the experimental data is marked with squares and the fitting used to calculate zT is a solid line, (B) Seebeck coefficient of select $Eu_{5-x}A_xSn_2As_6$ (A = K, La) compounds.

Table 1. Room temperature resistivity of $Eu_{5-x}A_xSn_2As_6$ (A = K, La) compounds.

Composition	~ RT Resistivity (mΩ-cm)
$Eu_5Sn_2As_6$	462
$Eu_{4.975}K_{0.025}Sn_2As_6$	134
$Eu_{4.95}K_{0.05}Sn_2As_6$	115
$Eu_{4.9}K_{0.1}Sn_2As_6$	90
$Eu_{4.85}K_{0.15}Sn_2As_6$	42
$Eu_{4.99}La_{0.01}Sn_2As_6$	2504
$Eu_{4.9}La_{0.1}Sn_2As_6$	1837
$Eu_{4.85}La_{0.15}Sn_2As_6$	52
$Eu_{4.8}La_{0.2}Sn_2As_6$	25

The most impactful set of data for these materials is the Seebeck coefficient, **Figure 4B**. For the K-substituted samples the Seebeck coefficient follows with the similar trend that was experienced with the *p*-type doping of the similar $Ca_5Ga_2As_6$ structure type.[9,22–24] The transition to *n*-type no longer occurs and the onset of bipolar conduction shifts to higher temperature. The La-substituted sample has a Seebeck coefficient that is fully *n*-type across the entire temperature regime.

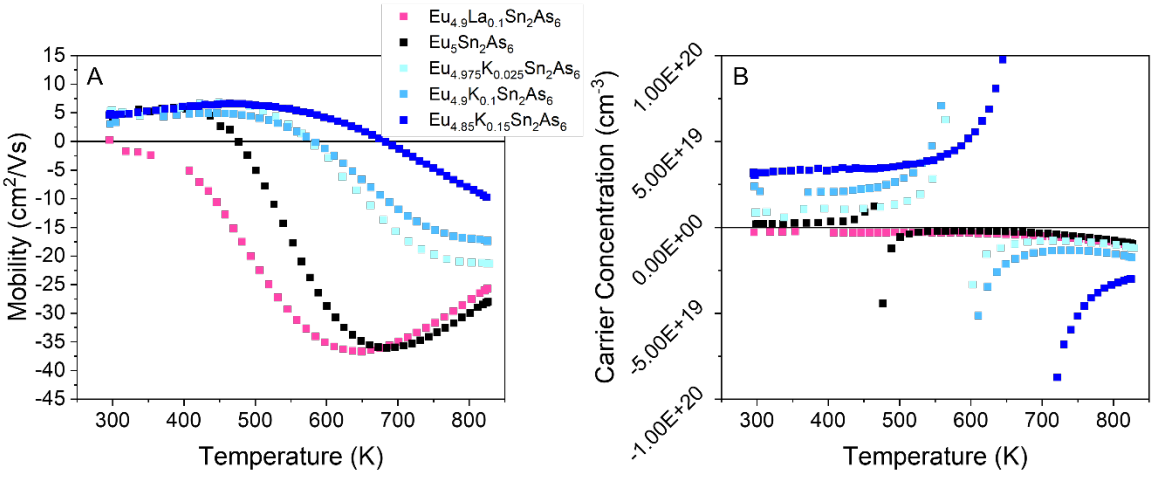

Figure 5. (A) Carrier concentration of select $Eu_{5-x}A_xSn_2As_6$ (A = K, La) compounds, (B) Mobility of select $Eu_{5-x}A_xSn_2As_6$ (A = K, La) compounds.

The mobility versus temperature of the materials is provided in **Figure 5A**. The mobility of the K-substituted materials is detrimentally impacted by the increasing K concentration; however, the parent compound and the La-substituted samples have excellent mobility in the high temperature regime.

The carrier concentrations of the materials are illustrated in **Figure 5B.** Unsubstituted $Eu_5Sn_2As_6$ is a *p*-type semiconductor at room temperature with a sharp transition to *n*-type at ~450 K in the carrier concentration and seen at ~650 K in the Seebeck measurement, **Figure 4B**. The high-temperature measurements illustrate thermally active bipolar transport with the asymptotic curvature of the carrier concentration being an artifact in the Hall voltage typical within Hall analysis when the single carrier type approximation breaks down. The substitution of K into $Eu_5Sn_2As_6$ shifts the *p*-type to *n*-type transition to higher temperatures with increasing K concentration shifting the onset of bipolar transport. Additionally, the carrier concentration is increased with K concentration, as expected. The carrier concentration of the La-substituted sample is *n*-type across the entire measured temperature range. This is indicative of the La-doping into the structure. This mechanism can also be used to understand the initial increase in resistivity and the subsequent decrease with additional electrons from the substitution of La into $Eu_5Sn_2As_6$. As the initial electrons are added the intrinsic defects are reduced, filling the valence band, increasing the resistivity. Once enough La is introduced the additional e^- provided by La begins adding to the conduction band and a decrease in resistivity is seen. This mechanism is consistent with the density of states and crystal orbital Hamilton population proposed by Wang et al.[1] and other *n*-type Zintl thermoelectric phases.[15]

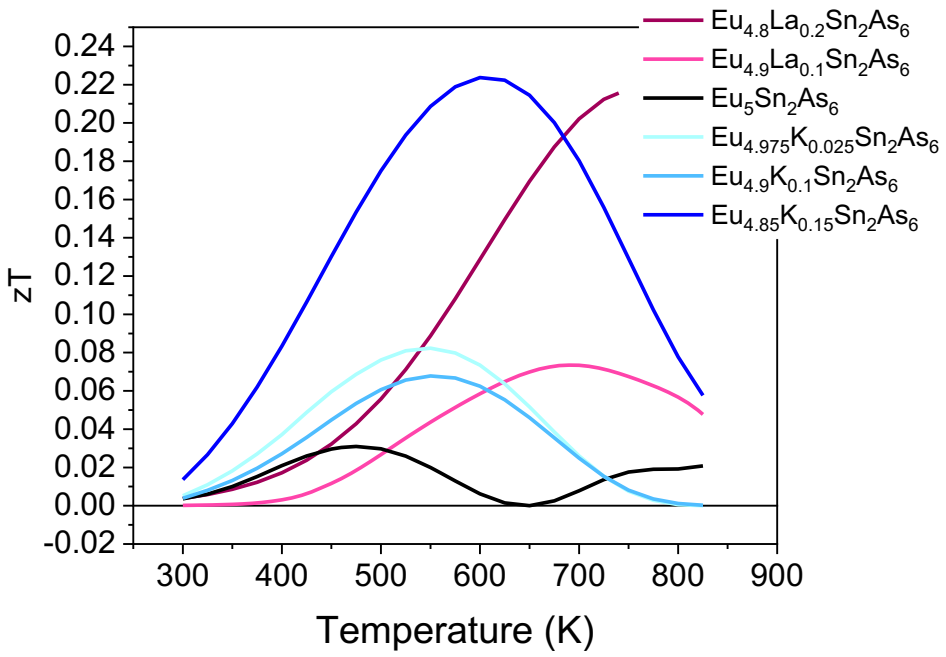

Figure 6. *zT* of select $Eu_{5-x}A_xSn_2As_6$ (A = K, La) compounds.

The *zT* of the material was calculated from the above fitted data, **Figure 6**. The maximum *zT* is 0.22 at 600 K for $Eu_{4.85}K_{0.15}Sn_2As_6$; however, all samples have been improved over the parent sample. The $Eu_{4.8}La_{0.2}Sn_2As_6$ sample has a maximum *zT* 0.22 at 740 K.

Summary

The substitution of K and La in the Zintl phase $Eu_5Sn_2As_6$ to form *p*-type and *n*-type semiconducting properties has been investigated. This structure type is of interest for the thermoelectric properties and this composition is a rare example of a Zintl phase that can be doped either *p*- or *n*-type. The samples were prepared from the elements and heat treated, consolidated in the dense pellets for measurements. Temperature dependent transport properties were measured. The substitution of K for Eu in $Eu_5Sn_2As_6$ shifts the transition from *p*- to *n*-type carriers to higher temperature systematically as a function of *x*. The substitution of La for Eu in $Eu_5Sn_2As_6$ removes the transition from *p*- to *n*-type over

the temperature range and provides an all *n*-type semiconductor. $Eu_{5-x}K_xSn_2As_6$ shows a maximum *zT* of 0.22 at 600 K for the composition $Eu_{4.85}K_{0.15}Sn_2As_6$. $Eu_{4.8}La_{0.2}Sn_2As_6$ shows promise as a new *n*-type Zintl phase with a maximum *zT* of 0.22 at 740 K.

Author Information

Corresponding Author* E-mail: smkauzlarich@ucdavis.edu.
ORCID
Susan M. Kauzlarich: 0000-0002-3627-237X
Kasey P. Devlin: 0000-0002-2633-7029

Notes

The authors declare no competing financial interest.

Acknowledgements

We thank NSF DMR-2001156 for funding. Some of the thermoelectric measurements were performed in part at the Jet Propulsion Laboratory, California Institute of Technology under contract with the National Aeronautics and Space Administration.

Supporting Information

The supporting information contains extended PXRD patterns and Rietveld refinement statistics.

References

(1) Wang, J.; Xia, S. Q.; Tao, X. T. $A_5Sn_2As_6$ (A = Sr, Eu). Synthesis, Crystal and Electronic Structure, and Thermoelectric Properties. *Inorg. Chem.* **2012**, *51* (10), 5771–5778.

(2) Eisenmann, B.; Jordan, H.; Schafer, H. Phasen Im Grenzbereich Der ZintlKonzeption: Zur Kenntnis Von $Sr_5Sn_2P_6$ UND SrSnP. *J. Less-Common Met.* **1986**, *116*, 251–258.

(3) Luo, D. B.; Wang, Y. X.; Yan, Y. L.; Yang, G.; Yang, J. M. The High Thermopower of the Zintl Compound $Sr_5Sn_2As_6$ over a Wide Temperature Range: First-Principles Calculations. *J. Mater. Chem. A* **2014**, *2* (36), 15159–15167.

(4) Eisenmann, B.; Jordan, H.; Schafer, H. $Ca_5Sn_2As_6$, Das Erste Inoarsenidostannat(IV). *Z. Anorg. Allg. Chem.* **1985**, *530*, 74–78.

(5) Verdier, P.; L'Haridon, P.; Maunaye, M.; Laurent, Y. Etude Structurale de $Ca_5Ga_2As_6$. *Acta Cryst.* **1976**, B*32* (3), 726–728.

(6) Cordier, G.; Schäfer, H.; Stelter, M. Ca_3AlSb_3 Und $Ca_5Al_2Bi_6$, Zwei Neue Zintlphasen Mit Kettenförmigen Anionen. *Z. Naturforsch.* **1984**, *39B*, 727–732.

(7) Cordier, G.; Steher, M. $Sr_5Al_2Sb_6$ Und $Ba_5In_2Sb_6$: Zwei Neue Zintlphasen Mit Unterschiedlichen Bänderanionen. *Z. Naturforsch.* **1988**, *43B* (4), 463–466.

(8) Childs, A. B.; Baranets, S.; Bobev, S. Five New Ternary Indium-Arsenides Discovered. Synthesis and Structural Characterization of the Zintl Phases $Sr_3In_2As_4$, $Ba_3In_2As_4$, $Eu_3In_2As_4$, $Sr_5In_2As_6$ and

$Eu_5In_2As_6$. *J. Solid State Chem.* **2019**, *278*, 120889.

(9) Zevalkink, A. Chain-Forming Zintl Antimonides as Novel Thermoelectric Materials, California Institute of Technology, 2013.

(10) Yeon, S.; Shin, S.; Jo, H.; Thi, N. Le; Moon, D.; Kim, D. H.; Ok, K. M.; You, T. S. P-Type to n-Type Conversion through the "Bypass" Phase Transition in the Zintl-Phase Thermoelectric Materials. *Chem. Mater.* **2021**, *33* (17), 6761–6773.

(11) Toberer, E. S.; May, A. F.; Scanlon, C. J.; Snyder, G. J. Thermoelectric Properties of p -Type LiZnSb: Assessment of Ab Initio Calculations. *J. Appl. Phys.* **2009**, *105* (6), 063701.

(12) Liu, Z.; Mao, J.; Peng, S.; Zhou, B.; Gao, W.; Sui, J.; Pei, Y.; Ren, Z. Tellurium Doped N-Type Zintl $Zr_3Ni_3Sb_4$ Thermoelectric Materials: Balance between Carrier-Scattering Mechanism and Bipolar Effect. *Mater. Today Phys.* **2017**, *2*, 54–61.

(13) Gorai, P.; Goyal, A.; Toberer, E. S.; Stevanović, V. A Simple Chemical Guide for Finding Novel N-Type Dopable Zintl Pnictide Thermoelectric Materials. *J. Mater. Chem. A* **2019**, *7* (33), 19385–19395.

(14) Cordier, G.; Ochmann, H. Crystal Structure of Potassium Tecto-Tetraanti- Monidogallate , $KGaSb_4$. *Z. Kristallogr. Cryst. Mater.* **1991**, *195*, 306–307.

(15) Ortiz, B. R.; Gorai, P.; Stevanović, V.; Toberer, E. S. Thermoelectric Performance and Defect Chemistry in N-Type Zintl $KGaSb_4$. *Chem. Mater.* **2017**, *29* (10), 4523–4534.

(16) Cordier, G.; Ochmann, H. Crystal Structure of Potassium Tecto-Tetraanti- Monidoaluminate, $KAlSb_4$. *Z. Kristallogr. Cryst. Mater.* **1991**, *195*, 308–309.

(17) Ortiz, B. R.; Gorai, P.; Krishna, L.; Mow, R.; Lopez, A.; McKinney, R.; Stevanović, V.; Toberer, E. S. Potential for High Thermoelectric Performance in N-Type Zintl Compounds: A Case Study of Ba Doped $KAlSb_4$. *J. Mater. Chem. A* **2017**, *5* (8), 4036–4046.

(18) Tamaki, H.; Kanno, T.; Sakai, A.; Takahashi, K.; Yamada, Y. Thermoelectric Properties and Electronic Transport Analysis of $Zr_3Ni_3Sb_4$-Based Solid Solutions. *J. Appl. Phys.* **2015**, *118* (5), 055103.

(19) Lee, J.; Sa, H.; Jo, H.; Moon, D.; Ok, K. M.; You, T.-S. Site-Selective n -Type "Heavy" Rare-Earth-Metal Doping in the Complex Zintl Phase $Ca_{11-x}RE_xSb_{10-y}$ (RE = Tb, Dy, Ho, Er, Tm) . *Cryst. Growth Des.* **2020**, 0–8.

(20) Zoltan, D.; Wood, C.; Stapfer, G. Measurement of Seebeck Coefficient Using a Light Pulse. *Proc. Intersoc. Energy Convers. Eng. Conf.* **1984**, *719*, 2241–2243.

(21) Borup, K. A.; Toberer, E. S.; Zoltan, L. D.; Nakatsukasa, G.; Errico, M.; Fleurial, J. P.; Iversen, B. B.; Snyder, G. J. Measurement of the Electrical Resistivity and Hall Coefficient at High Temperatures. *Rev. Sci. Instrum.* **2012**, *83* (12), 123902.

(22) Zevalkink, A.; Swallow, J.; Ohno, S.; Aydemir, U.; Bux, S.; Snyder, G. J. Thermoelectric Properties of the $Ca_5Al_{2-X}In_xSb_6$ Solid Solution. *Dalton Trans.* **2014**, *43* (42), 15872–15878.

(23) Zevalkink, A.; Swallow, J.; Snyder, G. J. Thermoelectric Properties of Zn-Doped $Ca_5In_2Sb_6$. *Dalton Trans.* **2013**, *42* (26), 9713–9719.

(24) Toberer, E. S.; Zevalkink, A.; Crisosto, N.; Snyder, G. J. The Zintl Compound $Ca_5Al_2Sb_6$ for Low-Cost Thermoelectric Power Generation. *Adv. Funct. Mater.* **2010**, *20* (24), 4375–4380.